Pharm Res
DOI 10.1007/s11095-012-0770-0

RESEARCH PAPER

Surface-Engineered Nanoliposomes by Chelating Ligands for Modulating the Neurotoxicity Associated with β-Amyloid Aggregates of Alzheimer's disease

Maluta S. Mufamadi • Yahya E. Choonara • Pradeep Kumar • Girish Modi • Dinesh Naidoo • Valence M. K. Ndesendo • Lisa C. du Toit • Sunny E. Iyuke • Viness Pillay

Received: 9 December 2011 / Accepted: 30 April 2012

ABSTRACT

Purpose To develop chelating ligand-bound nanoliposomes (NLPs) for the prevention and reversal of β-Amyloid (Aβ) aggregation associated with promoting neurotoxicity in Alzheimer disease (AD).

Methods Four different chelating ligands (CuAc, EDTA, histidine and ZnAc) were surface-engineered onto NLPs using either covalent or non-covalent conjugation. Successful conjugation of chelating ligands onto the surface of NLPs was confirmed by characterization studies: SEM, TEM and FTIR analysis. Chelation energetics of EDTA with Cu(II)/Zn(II)-Aβ(10-21) and nanoformation of emulsified polymers were computed and corroborated with experimental and analytical data using chemometric molecular modeling.

Results The modified NLPs produced were spherical in shape, 127–178 nm in size, with polydispersity index from 0.217–0.920 and zeta potential range of −9.59 to −37.3 mV. Conjugation efficiencies were 30–76 %, which confirmed that chelating ligands were attached to the NLP surface.

Conclusions *In vitro* and *ex vivo* results elucidated the effectiveness of chelating ligand-bound NLPs for prevention of CuAβ(1-42) or ZnAβ(1-42) aggregate buildup associated with neurotoxicity in PC12 neuronal cells, as well as promotion of intracellular uptake in the presence of Cu(II) or Zn(II) metal ions.

KEY WORDS Alzheimer's disease · chelating ligands · surface-engineered nanoliposomes · targeted delivery · β-amyloid neurotoxicity

INTRODUCTION

Alzheimer's disease (AD) is the most common neurodegenerative disorder (ND) (1–3). It is characterized by a progressive decline of cognitive function, complete loss of memory, deterioration of visual capacity and the ability to function independently (1). Recent studies by Brookmeyer and coworkers (2), estimated that there are approximately 26 million people suffering with AD worldwide and an estimated increase of 5–16 million people that will be affected by AD in the United States by the year 2050. Although the development of AD is not fully understood, it is a condition associated with the formation of extracellular neurotoxic senile plaques and neurofibrillary tangles comprising hyperphosphorylated tau proteins (3,4). Mounting evidence supports the fact that senile plaques are caused by 40 or 42 amino acid peptides which are generated by proteolytic

M. S. Mufamadi · Y. E. Choonara · P. Kumar · L. C. du Toit · V. Pillay (✉)
Faculty of Health Sciences, Dept. of Pharmacy & Pharmacology
University of the Witwatersrand Parktown
2193 Johannesburg, South Africa
e-mail: viness.pillay@wits.ac.za

G. Modi
Faculty of Health Sciences, Dept. of Neurology
University of the Witwatersrand Parktown
2193 Johannesburg, South Africa

D. Naidoo
Faculty of Health Sciences, Dept. of Neurosurgery
University of the Witwatersrand Parktown
2193 Johannesburg, South Africa

V. M. K. Ndesendo
School of Pharmacy & Pharmaceutical Sciences
St. John's University of Tanzania, Dodoma, Tanzania

S. E. Iyuke
School of Chemical & Metallurgical Engineering
University of the Witwatersrand Private Bag 3, Wits
2050 Johannesburg, South Africa

Published online: 15 May 2012

cleavage (β and γ secretase enzymes) of the β-amyloid (Aβ) precursor glycoprotein (APP) (5). On one hand, there is considerable evidence that extracellular soluble Aβ peptide has to undergo a process of aggregation with biological metals ions (such as zinc and copper ions) in order to form insoluble Aβ peptide which is substantiated to promote neurotoxic Aβ peptide forms of plaques in AD (Fig. 1) (6–9). This condition is greatly influenced by a breakdown in the homeostatic mechanisms resulting in abnormal or overexpressed biological transition metal ions such as zinc and copper ions that are coordinated with the histidine residues in the AP core or Aβ deposits (10–13).

Several therapeutic metal chelators or chelating agents (such as 5-chloro-7-iodo-8-hydroxyquinoline (clioquinol) (CQ), ethylenediaminetetraacetic acid (EDTA), histidine residues and zinc acetate (ZnAc) that can restore biometal homeostasis and prevent/reverse Aβ aggregation, have been explored in both *in vitro* and *in vivo* studies (10,14). A study conducted by Opazo and co-workers demonstrated that the beneficial effects of CQ is that it is able to reduce the size and number of Aβ plaques in transgenic AD in mice (15). In another study by Bush and co-worker (16), it was revealed that CQ restored intracellular zinc and copper ions through ionophore processes in which CQ:Cu or CQ:Zn complexes mediated the transport of metal ions into the cell. The study also confirmed that CQ:Cu or CQ:Zn intracellular complexes induced the up-regulation of matrix metalloproteases ultimately promoting the digestion of amyloid oligomers. EDTA is most widely used as a chelating agent due to its claw-like molecular structure that binds to transition metals with a high affinity constant to form EDTA complexes (such as Cu-EDTA and Zn-EDTA) (17). Chelation therapy with EDTA has been approved by the US Food and Drug Administration (FDA) for the management of symptoms associated with cardiovascular disease, more recently with AD (18,19). In another chelation form of therapy, histidine residues showed to have anti-copper or anti-zinc activity in AD (20). In a study conducted by Chikha and co-workers (21) it was demonstrated that surface engineered lipid-based carriers with histidine-rich peptide or protein improved transition metal bindings. In addition, the chelating ligand zinc acetate (ZnAc) has been validated as the compound of choice for the treatment and management of Wilson's disease (WD) (22). ZnAc accomplishes its effectiveness as a chelating ligand by means of blocking copper absorption which ultimately induces hepatic metallothionein synthesis thus resulting in the alleviation of the toxic effects of copper in intestinal mucosal cells (23). In other countries particularly the United States and a few European countries, ZnAc is currently available as prescription medicine for WD under the tradename Galzin® and Wilzin® respectively (24). Figure 1 provides a schematic depicting the process of Aβ aggregate formation with metal ions Cu(II) and Zn(II) in AD (7).

Despite these potential chelating agents (i.e. histidine, EDTA and ZnAc), clinical improvement or management of diseases in the CNS such as AD is hampered by poor absorption, toxic side-effects and the difficulty to bypass the highly restrictive Blood–brain Barrier (BBB) thus hindering further investigation (25). In order to avoid these disadvantages while improving delivery efficacy and reducing toxicity associated with side-effects, sterically stabilized Nanoliposomes (NLPs) have been developed as potential delivery vehicles for such CNS conditions (26–30). NLPs are prominent candidates due to their unique characteristics such as low toxicity, capability of crossing the BBB and the ease by which

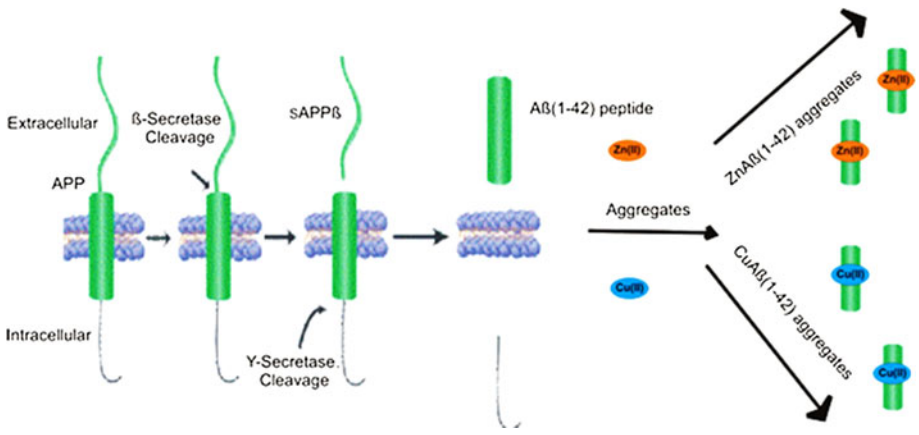

Fig. 1 Schematic depicting the process of beta aggregates formation with metal ions (Cu(II) and Zn(II)) in Alzheimer's disease. (adapted from Citron *et al.*, (7)).

they can be manipulated within their surface membrane (18,21,31–35). This unique approach of chelating ligand delivery systems utilizing NLPs could significantly advance the efficacy of chelating agents in the management of AD.

Therefore the aim of this study was to develop novel NLPs that were surface-engineered with chelating ligands such as EDTA, histidine and ZnAc. The chelating ligands conjugated on the surface of NLPs using either covalent or non-covalent procedures were validated. In addition, the possibility of the modified chelating ligand-bound NLPs to resolubilize or disaggregate ZnAβ (1-42) or CuAβ (1-42) aggregates using a Label Guard™ Microliter Cell NanoPhotometer™ (Implen GmbH, Munich, Germany) was investigated via quantifying the concentration of proteins. The study also attempted to prove that the modified chelating ligand-bound NLPs (practically EDTA, histidine and ZnAc) rendered resolubilization either through ZnAβ(1-42) or CuAβ(1-42) aggregates *in vitro*. *Ex vivo* experiments were undertaken to demonstrate that ZnAβ(1-42) or CuAβ(1-42) aggregates induced neurotoxicity to PC12 neuronal cells. Furthermore, it was confirmed that the neurotoxicity associated with Aβ aggregates was reversed after employing the modified chelating ligand-bound NLPs. The modified NLPs were also assessed in terms of the chelating ligands (EDTA, histidine and ZnAc) to significantly facilitate intracellular delivery with the influence of Cu(II) and Zn(II) metal ions *ex vivo*. Molecular Mechanics Energy Relationships (MMER) were employed to corroborate the experimental findings by exploring the spatial disposition of energy minimized molecular structures.

MATERIALS AND METHODS

Materials

Phospholipids (1,2 distearoyl-sn-glycero-3-phosphocholine) (DSPC), cholesterol (CHOL), phosphatidylethanolamine distearoyl methoxypolyethyleneglycol conjugate (DSPE-mPEG2000COOH), phosphatidylethanolamine rhodamine-B triethylamine salts (Rh-DSPE), flourescein isothiocyanate (FITC), ethylenediaminetraacetic acid (EDTA), L-histidine, β-amyloid (1-42) synthetic peptide, N,N′-dicyclohexylcarbodiimide (DCC) and *N*-hydroxysulfosuccinimide (NHS) were all purchased from Sigma-Aldrich (St. Louise, MO, USA). Zinc acetate (ZnAc), copper acetate (CuAc), copper chloride ($CuCl_2$) and zinc chloride ($ZnCl_2$) were purchased from Saarchem (Pty) Ltd. (Brakpan, South Africa). Membrane filters (0.22 μm) were purchased from Millipore® (Billerica, MA, USA). The CytoTox-Glo™ Cytotoxicity Assay which measures cell viability was purchased from Promega Corporation (Madison, WI, USA). All other chemicals used in the experiments were of analytical grade and were employed as purchased.

Methods

Preparation of the Nanoliposomes

Nanoliposomes (NLPs) were prepared using an adapted reverse-phase evaporation technique developed by Takizawa and co-workers (36). Briefly, DSPC, CHOL and DSPE-mPEG conjugate (with rhodamine or FITC labeled markers) were dissolved in an organic solvent phase of chloroform/methanol (9:1). Pluronic F68 ($5\%^{w}/_{v}$) was then added as a surfactant (Table I). The mixture was then blended with a probe sonicator (Sonics & Materials, Inc., CT, USA) followed by solvent removal by rotary evaporation (Rotavapor® RII, Büchi Labortechnik AG, Switzerland) maintained at 60°C to obtain a thin lipid film. The appropriate volume of phosphate buffered saline (PBS) (preheated at 60°C) was added and the vessel vigorously agitated on a rotary mixer to produce multilamellar vesicles (MLVs). The MLVs were then sonicated at 60°C for 5 min to produce unilamellar liposomes. Size distribution was obtained by gradually extruding through a 0.22 μm pore size polycarbonate membrane filter and the samples obtained were allowed to stabilize at 4°C until further analysis.

Surface Modification of the Nanoliposomes Using Chelating Ligands

NLPs with DSPE-mPEG-COOH were used to conjugate the chelating ligand using either covalent or non-covalent conjugation procedures (37–40). Briefly, activated NLPs (with 45 mg/mL NHS and 60 mg/mL DCC) and chelating ligands (65 mM of histidine and 34 mM of EDTA) were conjugated using a covalent procedure. A non-covalent conjugation procedure was employed for surface modification of NLPs with ZnAc (50 mM) and CuAc (82 mM) in PBS buffer at pH 7.4. The reactions were allowed to agitate continuously overnight at room temperature. Organic solvent was precipitated by rotary evaporation (Rotavapor® RII, Büchi Labortechnik AG, Switzerland) maintained at 60°C for 3 h. Finally, the reactions mixtures either covalent or non-covalent conjugated were extensively dialyzed

Table I Compositions of Nanoliposomes Formulations with Chelating Ligands

F#	DSPC/CHOL/DSPE/P68 (m/m/m/m)	CuAc (mM)	ZnAc (mM)	L-His (mM)	EDTA (mM)
Unmodified NLPs	55/62.5/12.5/5	0	0	0	0
1	55/62.5/12.5/5	50	0	0	0
2	55/62.5/12.5/5	0	82	0	0
3	55/62.5/12.5/5	0	0	65	0
4	55/65.5/12.5/5	0	0	0	34

(Snakeskin^{TM} Pleated Dialysis Tubing, 10,000 MWCO; Sigma-Aldrich; St. Louise, MO, USA) against PBS at pH 7.4 for 48 h to remove unconjugated or unbound chelating ligands.

Evaluation of the Conjugation Efficiency of Chelating Ligands on the Nanoliposomes Surface

Evaluation of the conjugation efficiency of chelating ligands (CuAc, EDTA, histidine and ZnAc) on the surface of NLPs was conducted using a NanoPhotometer™ spectrophotometer (Implen GmbH, Munich, Germany). Briefly, 2 mL of 1 % Triton x100 in methanol was added to 4 mL solution of modified NLPs. The suspensions were allowed to react for 2 hour at 45°C in a laboratory oven. The absorbance of the final solution was read on a NanoPhotometer™ at λ_{max}= 220–245 nm (230 nm for CuAc and histidine, 220 nm for ZnAc and 245 nm for EDTA) against a blank sample of unmodified NLPs. The conjugation efficiency was used to confirm the total quantity of chelating ligands coupled or conjugated onto the surface of NLPs and was calculated using Eq. 1.

$$\text{Conjugation efficiency (\%)} = \frac{\text{Actual quantity of chelating ligand on NLPs}}{\text{Theoretical quantity of chelating ligand employed}} \times 100 \quad (1)$$

Determination of Size and Zeta Potential of the Modified Nanoliposomes

Determination of the average particle size, polydispersity index (Pdi) and zeta potential of unmodified NLPs and modified NLPs (with chelating ligands) were analyzed using a Zetasizer NanoZS instrument (Malvern Instruments (Pty) Ltd., Worcestershire, UK) at 25°C. All NLPs particle size and zeta potential measurements were performed in the same manner, whereby each sample was diluted (1 in 10) with deionized water using disposable cuvettes for each run (quartz cuvettes). Each test was performed in triplicate and the average value in each case was reported accordingly.

Chemical Structure Analysis of the Modified Chelating Ligand-Bound Nanoliposomes

FTIR spectroscopy was performed on the modified NLPs in order to characterize the potential interaction between the chelating ligands and the surface-conjugated NLPs. Samples were compressed into 1x13mm disks using a Beckmann Hydraulic Press (Beckman Instruments Inc., Fullerton, USA), and then analyzed at high resolution with wavenumbers ranging from 4,000–400 cm^{-1} on a Nicolet Impact 400D FTIR Spectrophotometer coupled with Omnic FTIR research grade software (Nicolet Instrument Corp., Madison, WI, USA).

Evaluation of the Surface Morphology and Architecture of the Modified Nanoliposomes

Scanning Electron Microscopy Examination. Scanning electron microscopy (SEM) (Jeol JSM-120, Tokyo, Japan) was undertaken to reveal the surface morphology of the NLPs. A small quantity of lyophilized NLPs and modified chelating ligand-bound NLPs were secured on a metallic sample stub and sputter-coated with a layer of carbon. Each sample was viewed under varying magnifications at an accelerating voltage of 20 kV.

Transmission Electron Microscopy Examination. Unmodified NLPs and modified chelating ligand-bound NLPs (with CuAc, EDTA, histidine or ZnAc) dispersions were diluted approximately 1:10 with PBS buffer at pH 7.4 and ultrasonicated at 37°C for 5 min. One drop of the diluted sample was placed on a carbon-coated copper grid for 5 min followed by removal of the excess liquid that was carried using a filter paper and air-dried. The films on the copper grid were examined using Transmission Electron Microscopy (TEM) (Jeol 1200 EX, Japan) at 10,000x magnification.

In Vitro Studies on the Formation of Aβ(1-42) Aggregates

To assess the effect of Cu(II) or Zn(II) metal ions on the formation of Aβ aggregates, *in vitro* analysis was performed as previously described (21). Briefly 5 mM of Aβ(1-42)

peptide was incubated with $CuCl_2$ (20 mM) and $ZnCl_2$ (20 mM) in 25 mM Tris/150 mM NaCl buffer (pH7.4; 37°C) for 24 h. Samples were then centrifuged (Optima® LE-80 K, Beckman, USA) at 10,000 rpm for 20 min. The supernatant aliquots were directly analyzed using a NanoPhotometer™ Spectrophotometer (Implen GmbH, Munich, Germany) at a λ_{max}=280 nm for total soluble Aβ(1-42) peptide percentage computation. All experiments were performed in triplicate.

Assessment of the Effect of the Modified Chelating Ligand-Bound NLPs on Resolubilization of Aβ(1-42) Peptides

To determine the resolubilization percentage of Aβ(1-42) peptides through chelation of the modified NLPs, CuAβ(1-42) or ZnAβ(1-42) aggregates were incubated with either unmodified or modified chelating ligand-bound NLPs (82 mM CuAc, 34 mM EDTA, 65 mM histidine and 50 mM ZnAc). Thereafter reaction mixtures in 0.5 % Triton X-100 in methanol were vortexed briefly and incubated at 45°C in a laboratory oven for 2 h. The samples were then centrifuged (Optima® LE-80K, Beckman, USA) at 10,000 rpm for 20 min. The supernatant aliquots were then analyzed using the Label Guard™ Microliter Cell of the NanoPhotometer™ (Implen GmbH, Munich, Germany) for computation of the protein concentration as a percentage. The total percent of Aβ(1-42) in the soluble fraction was performed in triplicate.

PC12 Neuronal Cell Culture Studies

PC12 neuronal cells were purchased from the Health Science Research Resources Bank (HSRRB, Osaka, Japan) (41). The cells were cultured in RPMI-1640 media (with L-glutamine and sodium bicarbonate) supplemented with 5 % fetal bovine serum, 10 % horse serum (both heat inactivated) and 1 % penicillin/streptomycin (Sigma-Aldrich; St. Louise, MO, USA). The cells were then maintained in an incubator (RS Biotech Galaxy, Irvine, UK) with a humidified atmosphere of 5 % CO_2 at 37°C.

Ex Vivo Neurotoxicity Assay of Metal Ions and Aβ1-40 Aggregates

Neurotoxicity on PC12 neuronal cells was detected by a CytoTox-Glo™ Cytotoxicity assay (Promega Co. Madison, USA). Since CytoTox-Glo™ cytotoxicity reagents contain the AAF-Glo Assay™ substrate and rLuciferase that cannot cross intact cell membranes, only external release protease (normal from dead cells) could cleave the proluminescent substrate which generated a luminescent signal from luciferase (42). Briefly, PC12 neuronal cells were incubated with ZnAβ(1-42) or CuAβ(1-42) aggregates at 37°C in a CO_2 incubator (RS Biotech Galaxy, Irvine, UK) for 24 h. An appropriate quantity of CytoTox-Glo™ reagent containing the substrate was added to each well as per the Promega Co. protocol. The cytotoxicity assay was performed by incubation of the CytoTox-Glo™ substrate with treated cells at room temperature for 15 min. The supernatant was collected through centrifuging (Optima® LE-80 K, Beckman, USA) at 1,800 rpm for 20 min. For cell viability studies, the pellet was further lysed with CytoTox-Glo™ buffer which was followed by incubation at room temperature for 15 min. Dead and live cell signals were measured by a luminometer (Victor™X3, Perkin Elmer Inc., USA).

Neurotoxicity Analysis of the Modified Chelating Ligand-Bound Nanoliposomes

The effect of modified chelating ligand-bound NLPs on neurotoxicity associated with Aβ aggregates was determined by the CytoTox-Glo™ Cytotoxicity assay as previously described. Briefly, PC12 neuronal cells were first exposed for 24 h to CuAβ(1-42) aggregates or ZnAβ(1-42) aggregates which is associated with neurotoxicity. This was followed by post-treatment with filtered sterile unmodified NLPs and modified chelating ligand-bound NLPs (82 mM CuAc, 34 mM EDTA; 65 mM histidine and 50 mM ZnAC) in RPMI 1649 media for 24 h at 37°C. Dead and live cell signals were analyzed using a luminometer (Victor™X3, Perkin Elmer Inc., USA).

Ex Vivo Uptake of the Modified Chelating Ligand-Bound Nanoliposomes by PC12 Neuronal Cells

The *ex vivo* uptake of the modified chelating ligand-bound NLPs was investigated on PC12 neuronal cells using Confocal Scanning Electron Microscopy (CSEM). PC12 neuronal cells were seeded at a density of 10,000 cells for 24 h in a 96-well culture plate. The cells were thereafter incubated with 20 mM $CuCl_2$ solution or 20 mM $ZnCl_2$ solutions in RPMI media for 2 h at 37°C in a CO_2 incubator. The *ex vivo* uptake capacity was performed on 50μL of fluorescent-labeled unmodified NLPs and 50μL of fluorescent-labeled NLPs surface modified with chelating ligands (CuAc, EDTA, histidine and ZnAc) previously diluted in culture medium. Cells were then incubated in RPMI 1640 free FBS and Horse serum for 4 h at 37°C in a CO_2 incubator. After 4 h of incubation, cells were re-suspended in fresh RPMI 1640 media supplemented with 10 % FBS and 5 % Horse serum. At 0, 6, 12, 18 and 24 h of incubation at 37°C under CO_2, the cells were washed four times with culture medium. The intracellular delivery efficiency was detected by a flourometer filter (Victor™X3 Perkin Elmer Inc. USA) at excitation and emission wavelengths of 450 nm and 482 nm, respectively. The bound fluorescent-labeled modified NLPs

with PC12 neuronal cells were visualized by Confocal Laser Scanning Microscopy.

Static Lattice Atomistic Simulations

All modeling procedures and computations, including energy minimizations in Molecular Mechanics (MM+), were performed using HyperChem™ 8.0.8 Molecular Modeling software (Hypercube Inc., Gainesville, FL, USA) and ChemBio3D Ultra 11.0 (CambridgeSoft Corporation, UK). DSPC and DSPC-PEG polymers were drawn using ChemBio3D Ultra in their syndiotactic stereochemistry as 3D models whereas the structure of $A\beta_{10–21}$ was built using the Sequence Editor Module on HyperChem 8.0.8. The structure of EDTA and CHOL were built with natural bond angles as defined by the software algorithm. The models were initially energy-minimized using MM+Force Field and the resulting structures were energy-minimized using the AMBER 3 (Assisted Model Building and Energy Refinements) Force Field. The conformer having the lowest energy was used to create the polymer-polymer and protein-chelator complexes. A complex of between molecules was assembled by disposing the molecules in a parallel way, and the same procedure of energy-minimization was repeated to generate the final models: DSPE-PEG/DSPC/CHOL, $A\beta_{10–21}$- Cu(II), $A\beta_{10–21}$- Cu(II)-EDTA, $A\beta_{10–21}$-Zn(II) and $A\beta_{10–21}$-Zn(II)-EDTA. Full geometrical optimization was performed in vacuum employing the Polak–Ribiere Conjugate Gradient algorithm until an RMS gradient of 0.001 kcal/mol was reached. Force Field options in the AMBER (with all H-atoms explicitly included) and MM+(extended to incorporate non-bonded limits, restraints, and periodic boundary conditions) methods were set as defaults (43).

RESULTS AND DISCUSSION

Conjugation Efficiency of Chelating Ligands on the Surface of the Nanoliposomes

The conjugation efficiencies of the modified chelating ligand-bound NLPs for CuAc, ZnAc, histidine and EDTA were determined using a NanoPhotometer™ spectrophotometer (Implen GmbH, Munich, Germany). Results indicated that the coupling efficiencies of the NLPs surface-modified with ZnAc, histidine and EDTA were 65 %, 76 %, and 68 % respectively (Table II). Comparably, the NLPs surface-modified with CuAc had a conjugation efficiency of 30 %. These results justify the desirable formation of the modified NLPs with chelating ligands which is suitable for enhancing the delivery of chelating agents into brain cells associated with AD.

Physicochemical Properties of the Targeted Nanoliposomes

Physicochemical characterization of the surface-modified NLPs (with CuAc, ZnAc, histidine and EDTA) such as the average particle size and zeta potential was measured using Dynamic Light Scattering (Zetasizer NanoZS, Malvern Instrument, UK). Table II shows the average particle size obtained for the unmodified NLPs. For the modified NLPs the results were as follows: i) 178 nm for CuAc-modified NLPs; ii) 130 nm for EDTA-modified NLPs; iii) 125 nm for histidine-modified NLPs and vi) 127 nm for ZnAc-modified NLPs. The Pdi value of the modified NLPs with chelating ligands (EDTA, histidine and ZnAc) ranged between 0.235–0.445, while the Pdi value for CuAc was 0.920. The zeta potential values were highly negatively distributed for all NLPs. For the unmodified NLP the zeta potential value was −28.7 mV while for modified NLPs it was −37.3 mV. NLPs modified with ZnAc had a zeta potential of −9.59 mV while for NLPs modified with histidine and EDTA the zeta potential values were −35.8 mV and −36.1 mV respectively (Table II). Worth noting is that when NLPs were modified with CuAc, the zeta potential decreased from been a highly negative charge toward a more neutral charge (−9.59 mV) (closer to neutrality). Overall, the results indicated that NLPs modified with chelating ligands contributed towards the increase of a net negative charge for the zeta potential value and a relative increase in particle size. Thus, the zeta potential of NLPs modified with chelating ligands such as EDTA, histidine and ZnAc served to confirm that the produced NLPs were physically stable.

Assessment of the Modified Nanoliposomes Chemical Structure Variations

FTIR spectra is one of the most powerful chemical analytical techniques used for analyzing IR spectra, vibration, and characteristics of chemical functional groups of phospholipids (44). FTIR spectra were generated to characterize the potential interactions of the NLPs and chelating ligands. As clearly depicted in Fig. 2, FTIR spectroscopy confirmed that there were molecular structural changes in the modified NLPs compared to the unmodified NLPs with chelating ligands. The FTIR spectra of modified NLPs displayed characteristic bond formations at the following bandwidths respectively, 1194.09 cm^{-1} (histidine), 1734.84 cm^{-1} and 1624.62 cm^{-1} (ZnAc), 1243.61 cm^{-1} (EDTA) and 1672.00, 1779.00 cm^{-1} as well as at 3222.85 cm^{-1} (CuAc). These peaks were absent in FTIR spectra of the unmodified NLPs. Overall, results showed that there were interactions between the NLPs and chelating ligands, which culminated into the formation of the novel modified NLPs that were surface-engineered.

Table II Physicochemical Characterization of the Unmodified and Modified Nanoliposomes

F#	DLS[a] size (nm)	Polydispersity Index (0–1)	Zeta Potential (mV)	Conjugation Efficiency (%)
Unmodified NLPs	100	0.217	−28.7	–
1	178	0.92	−9.59	30
2	127	0.445	−37.3	65
3	125	0.235	−35.8	76
4	130	0.251	−36.1	68

[a]Dynamic Light Scattering

Morphological Characterization of the Modified Nanoliposomes

TEM micrographs of modified chelating ligand-bound NLPs (with ZnAc, CuAc, histidine and EDTA) are shown in Fig. 3. TEM images revealed homogeneity and uniformity of the unmodified NLPs and modified NLPs suspension. The images also indicated that the unmodified NLPs and modified NLPs produced were of a nanosize range and were spherical in shape. SEM images of the modified NLPs presented with uniform surface morphology (Fig. 4). Results also confirmed that chelating ligands were surface-engineered onto the NLPs by either covalent or non-covalent bonding that contributed to the surface morphology.

In Vitro Metals Ions and Aβ (1-42) Resolubilization Assay

The modified chelating ligand-bound NLPs modulated with ZnAβ(1-42) or CuAβ(1-42) aggregates were confirmed

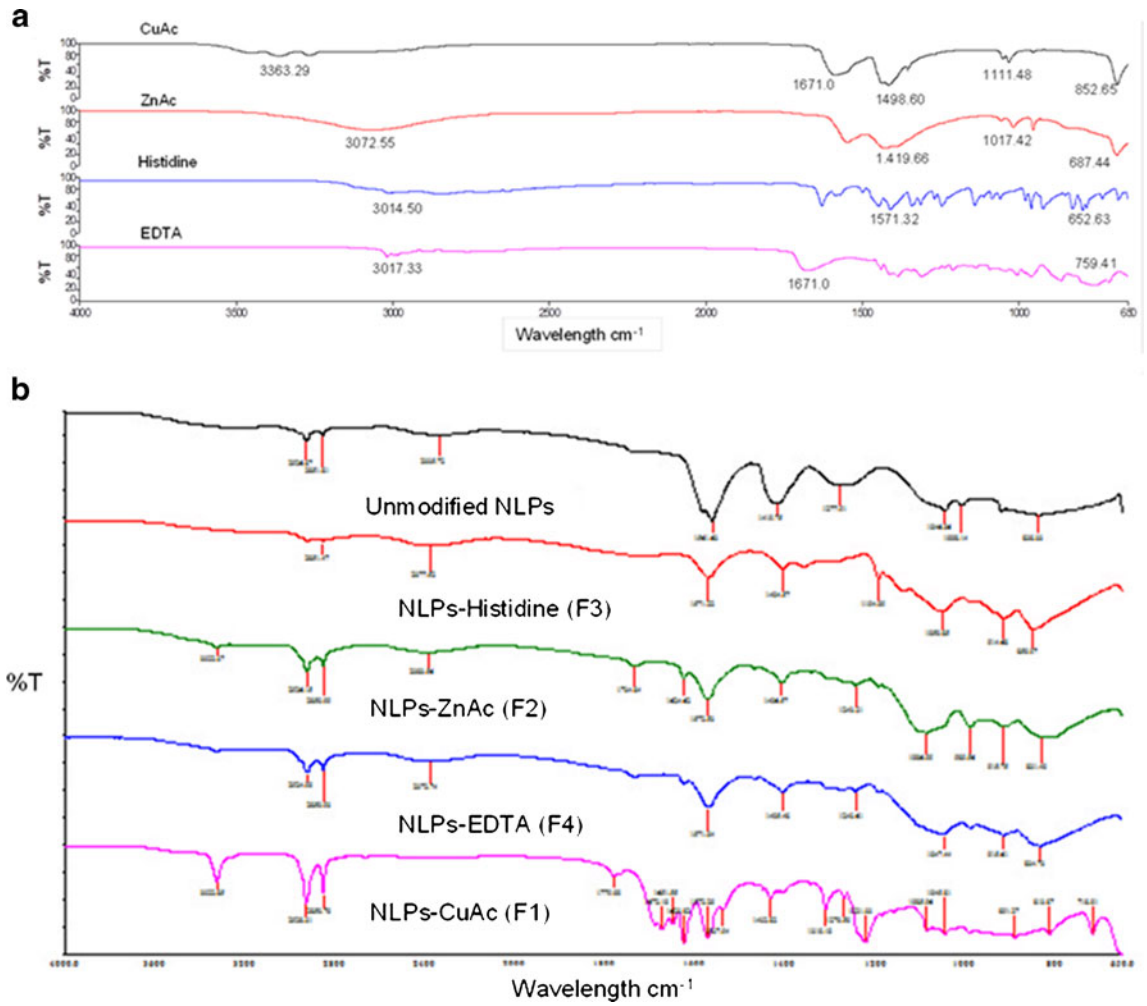

Fig. 2 FTIR spectra of (**a**) native CuAc, ZnAc, histidine and EDTA and (**b**) unmodified NLPs and surface-modified NLPs with histidine, ZnAc, EDTA and CuAc.

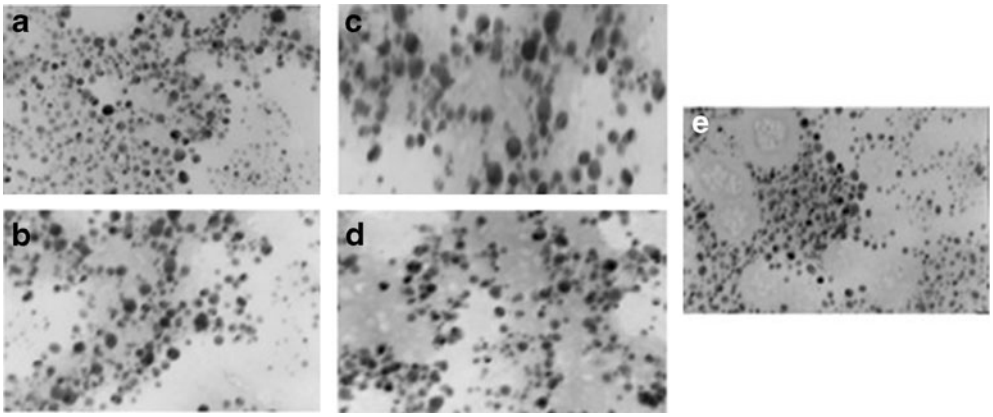

Fig. 3 TEM micrographs of (**a**) unmodified NLPs and modified NLPs with (**b**) ZnAc, (**c**) CuAc, (**d**) histidine and (**e**) EDTA.

in vitro (45). As shown in Fig. 5a, the percentage of soluble Aβ(1-42) peptide achieved by resolubilization of ZnAβ(1-42) aggregates with unmodified NLPs was 30 % while with modified NLPs this value increased to 40 % for CuAc-modified NLPs, 50 % for ZnAc-modified NLPs, 70 % for histidine-modified NLPs and 82 % for EDTA-modified NLPs. Fig. 5b, shows the percentages of soluble Aβ(1-42) achieved by resolubilization of CuAβ(1-42) aggregates with modified chelating ligand-bound NLPs. Unmodified NLPs showed 30 % resolubilization while modified NLPs were 42 % for CuAc-modified NLPs, 69 % for ZnAc-modified NLPs, 60 % for histidine-modified NLPs and 80 % for EDTA-modified NLPs. Unmodified NLPs and CuAc-modified NLPs did not show any significant effect on resolubilization of either ZnAβ(1-42) or CuAβ(1-42) aggregates after a 24 h reaction at 37°C. The high percentages of soluble Aβ(1-42) peptide confirmed that the surface-engineered NLPs with chelating ligands were effective in resolubilization/disaggregation of ZnAβ(1-42) and CuAβ(1-42) aggregates.

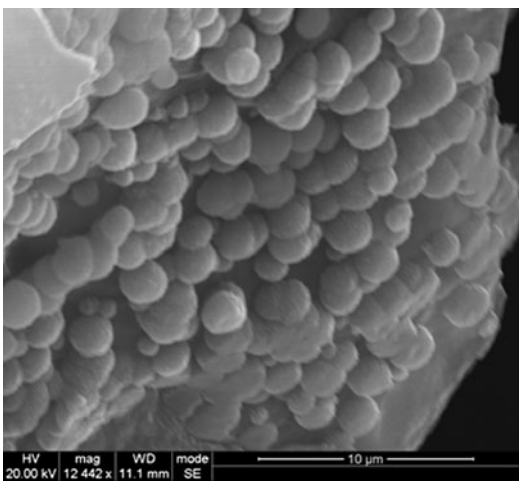

Fig. 4 Typical SEM image of the modified NLPs synthesized (magnification x12000).

Ex Vivo Neurotoxicity Assay of Metals Ions and Aβ1-40 Aggregates

The neurotoxicity profiles of metal ions [Zn(II) and Cu(II)], Aβ(1-42) peptide and ZnAβ(1-42) or CuAβ(1-42) aggregates on PC12 neuronal cells are shown in Fig. 6a. Cu(II) and Zn (II) ions showed low or no significant effect on cell viability when compared to untreated PC12 neuronal cells. At 5 mM Aβ(1-42) peptide concentration showed a small decrease in cell viability. However, when PC12 neuronal cells were exposed to ZnAβ(1-42) or CuAβ(1-(1-42) aggregates this resulted in a 60–70 % decrease of PC12 neuronal cell viability. These results confirmed that both ZnAβ(1-42) and CuAβ(1-42) aggregates induced neurotoxicity when exposed to PC12 neuronal cells. Metal ions such Cu(II) and Zn(II) as well as soluble Aβ(1-42) peptides showed no effects during *ex vivo* studies. This suggested that the metal ions and soluble Aβ(1-42) peptide were not responsible for the cytotoxicity or induced neurotoxicity on PC12 neuronal cells.

Effect of Modified Chelating Ligand-Bound Nanoliposomes on the Modulation of Neurotoxicity

Figure 6a–c depict the analytical data obtained for the determination of the effect of modified NLPs on the modulation of neurotoxicity of PC12 neuronal cells induced by ZnAβ(1-42) or CuAβ(1-42) aggregates. The analysis revealed non-restoration of cell viability after exposure to toxic ZnAβ(1-42) aggregates and thereafter treating with CuAc-bound NLPs (38 % cellular survival). In addition, the data showed an increase in cellular survival after treating neurotoxic PC12 neuronal with ZnAc-bound NLPs (50 % cellular survival), 66 % for histidine-bound NLPs and 68 % for EDTA-bound NLPs in *ex vivo* studies (Fig. 6b). Figure 6c, showed an increase in cell survival after exposure to cells with toxic CuAβ(1-42) aggregates and thereafter treated with modified chelating ligand-bound NLPs. ZnAc-,

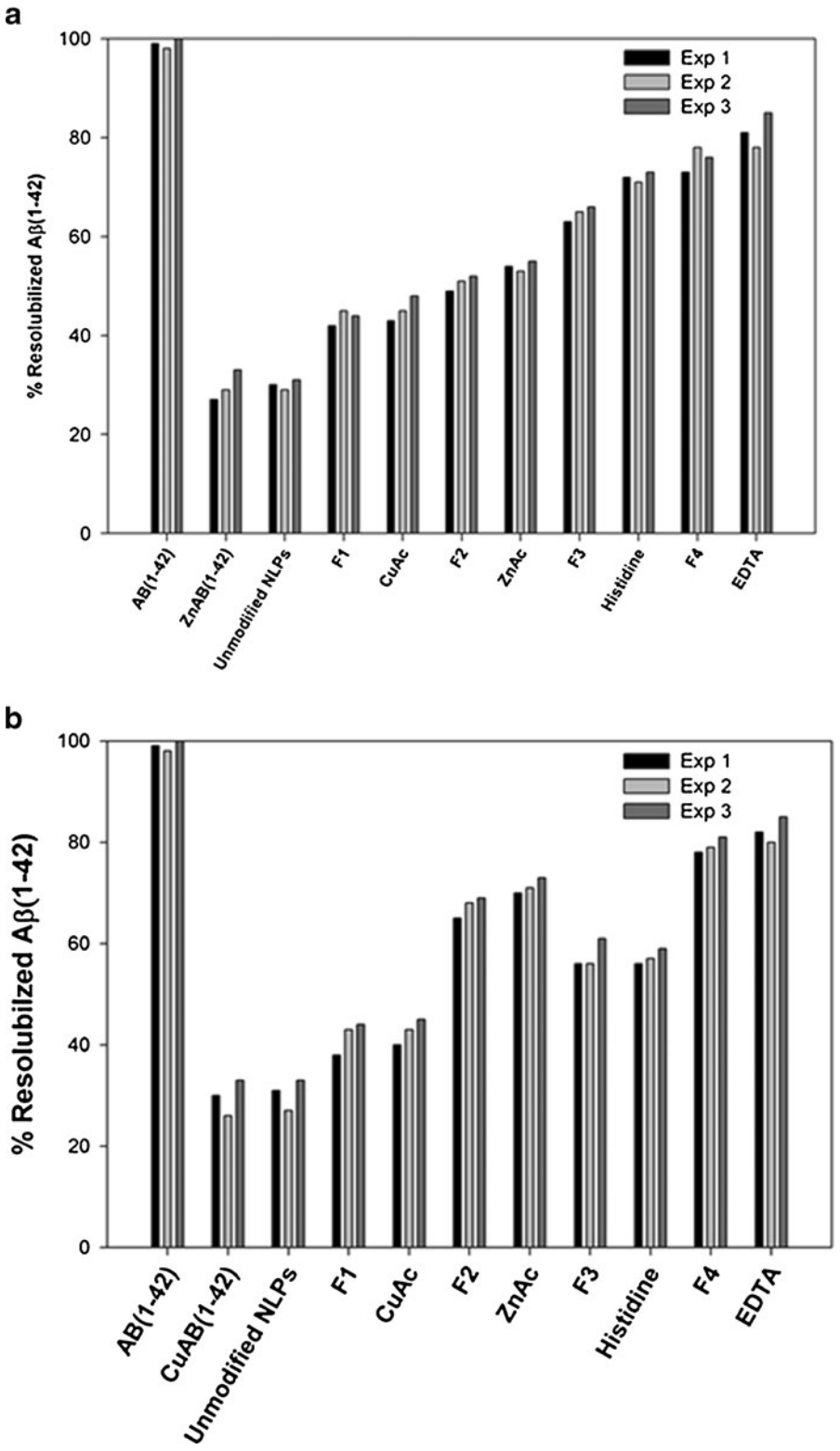

Fig. 5 Resolubilization of (**a**) ZnAβ(1-42) aggregates and (**b**) CuAβ(1-42) aggregates by modified NLPs.

histidine- and EDTA-bound NLPs exhibited 75 % cellular survival. However, when CuAc-bound NLPs was used to modulate neurotoxicity associated with toxic CuAβ(1-42) aggregates it did not show any significant effect (≤30 % cellular survival) on the restoration of cell viability. The data displayed the same trend as the *in vitro* study, which confirmed that the modified chelating ligand-bound NLPs, particularly ZnAc, histidine and EDTA were able to modulate both toxic CuAβ(1-42) and ZnAβ(1-42) aggregates *in vitro* and *ex vivo*.

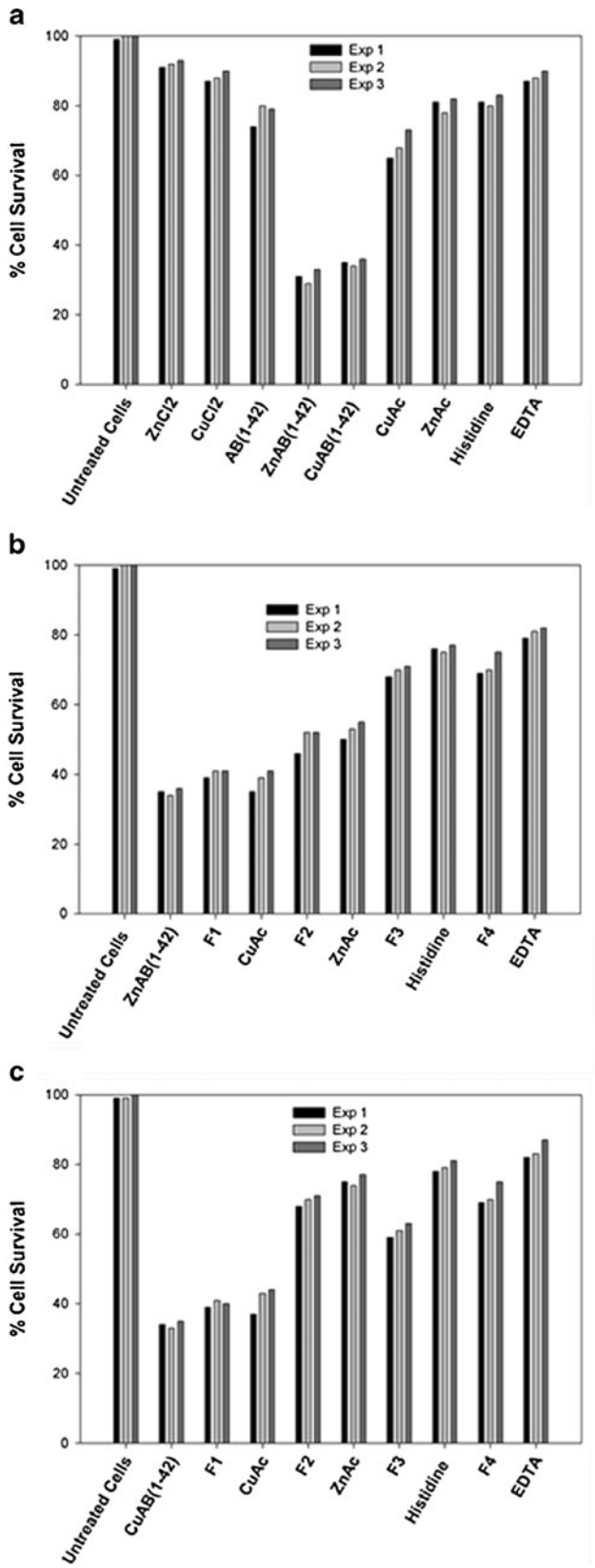

Fig. 6 (**a**) Effect of ZnAβ(1-42) and CuAβ(1-42) aggregates on cell viability, (**b**) effect of the modified NLPs on reversing neurotoxicity of ZnAβ (1-42) aggregates and (**c**) effect of the modified NLPs on neurotoxicity induced by CuAβ (1-42) aggregates.

Ex Vivo Uptake of Modified Chelating Ligand-Bound Nanoliposomes

To investigate the effect of the chelating ligands (EDTA, histidine and ZnAc) on mediated NLPs internalization, *ex vivo* samples were characterized by CSEM and fluorescence imaging (Victor™X3 Perkin Elmer Inc., USA). Analysis was performed in the presence of the metal ions Cu (II) or Zn(II) ions and results are shown in Figs. 7 and 8 (38). Results depicted low cellular uptake by the labeled NLPs in the presence of Cu(II) after 24 h. Modified NLPs (EDTA, histidine and ZnAc) were most efficiently taken up by PC12 neuronal cells in the presence of Cu(II) from 6–24 h (Fig. 7a). Figure 7b, shows that modified NLPs (with EDTA, histidine and ZnAc) were most efficiently taken up by PC12 cells when compared with unmodified NLPs in the presence of Zn(II). Unmodified NLPs and CuAc-bound NLPs showed no significant fluorescence activity in either Zn (II) or Cu(II). Confocal images did not show any significant difference on the modified NLPs by the cells since the results were field dependent (Fig. 8). Overall, these studies demonstrated that the modified chelating ligand-bound NLPs had a greater cellular uptake in either Zn (II) or Cu(II) ions. This data also indicated that intracellular uptake of NLPs was mediated by the surface-engineered chelating ligands on the NLPs.

Molecular Mechanics Energy Relationship (MMER) Analysis

MMER, a method for analytico-mathematical representation of potential energy surfaces, was used to provide evidence of the contributions of valence terms, non-covalent Coulombic terms, and non-covalent van der Waals interactions for chelation and nanostructure formation. The MMER model for potential energy in various molecular complexes can be written as shown in Eq. 2.

$$\mathbf{E_{molecule/complex}} = V_{\sum} = V_b + V_\theta + V_\varphi + V_{ij} + V_{hb} + V_{el} \ldots \quad (2)$$

Where, $V_{\sum}$ is related to total steric energy for an optimized structure, V_b corresponds to bond stretching contributions, V_θ denotes bond angle contributions, V_φ represents torsional contribution arising from deviations from optimum dihedral angles, V_{ij} incorporates van der Waals interactions due to non-bonded interatomic distances, V_{hb} symbolizes hydrogen-bond energy function and V_{el} denoted the electrostatic energy (46).

In the present study, the global energy relationships for the various complexes derived after assisted model building and energy refinements are shown in Eqs. 3–13.

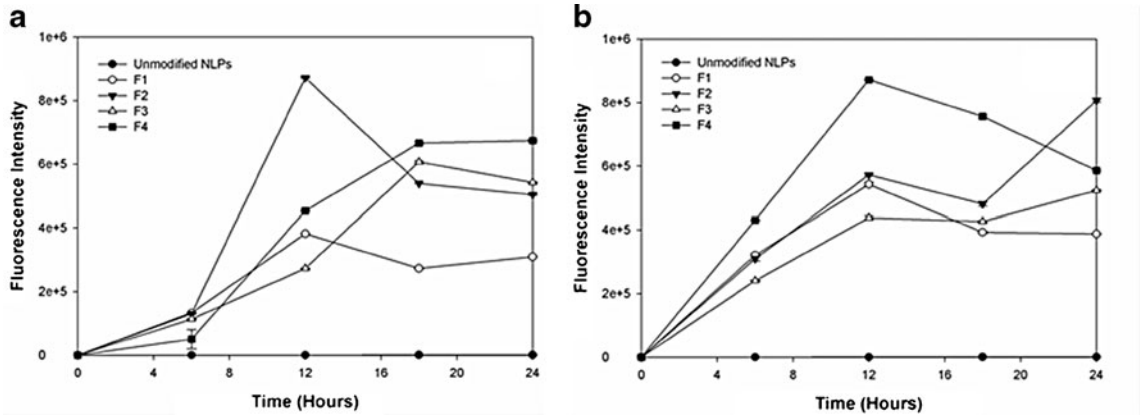

Fig. 7 Cellular uptake profiles of modified NLPs in the presence of (**a**) Cu(II) ions and (**b**) Zn(II) ions.

$$\mathbf{E_{DSPE-PEG}} = 57.33V_{\sum} = 2.49V_b + 17.35V_\theta + 42.18V_\varphi - 4.68V_{ij} - 0.005V_{hb}\ldots \quad (3)$$

$$\mathbf{E_{DSPC}} = 19.31V_{\sum} = 0.91V_b + 6.30V_\theta + 4.26V_\varphi + 7.85V_{ij} - 0.0007V_{hb}\ldots \quad (4)$$

$$\mathbf{E_{DSPE-PEG/DSPC}} = 49.36V_{\sum} = 2.43V_b + 16.32V_\theta + 39.76V_\varphi + -8.96V_{ij} - 0.19V_{hb}\ldots \quad \Delta\mathbf{E} = -27.273\ \text{kcal/mol} \quad (5)$$

$$\mathbf{E_{CHOL4}} = 152.984V_{\sum} = 7.56V_b + 45.76V_\theta + 56.68V_\varphi + 42.97V_{ij}\ldots \quad (6)$$

$$\mathbf{E_{DSPE-PEG/DSPC/CHOL}} = 149.83V_{\sum} = 9.65V_b + 62.29V_\theta + 102.22V_\varphi - 24.29V_{ij} - 0.032V_{hb}\ldots \quad \Delta\mathbf{E} = -79.786\ \text{kcal/mol} \quad (7)$$

$$\mathbf{E_{A\beta 10-21}} = -131.39V_{\sum} = 3.26V_b + 58.04V_\theta + 15.17V_\varphi - 18.41V_{ij} - 4.22V_{hb} - 185.23V_{el}\ldots \quad (8)$$

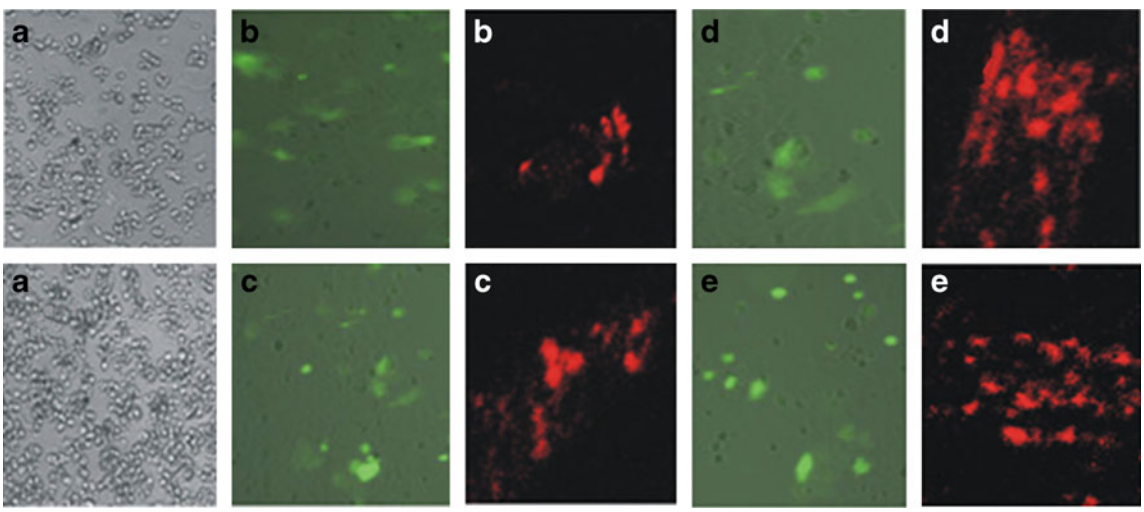

Fig. 8 Light and fluorescent microscopy analysis of PC12 cell line incubated in for 24 h (**a**) with labeled FTIC or rhodamine NLPs; (**b**) surface engineered with CuAc; (**c**) surface engineered ZnAc, (**d**) surface engineered EDTA and (**e**) surface-engineered histidine (magnification 100x).

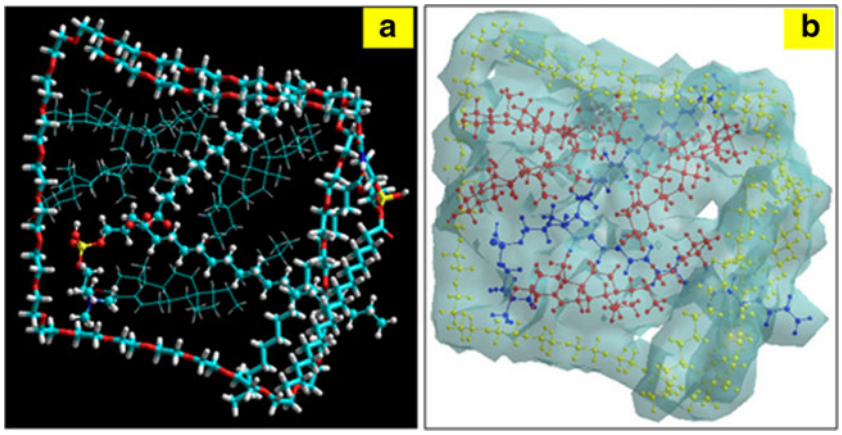

Fig. 9 Visualization of (**a**) geometrical preferences (color codes: C (*cyan*), O (*red*), N (*blue*, P (*yellow*) and H (*white*)); and (**b**) Connolly molecular electrostatic potential surfaces (color codes: DSPE-PEG (*yellow*), DSPC (*blue*) and CHOL (*red*)) in translucent display mode showcasing the nanoliposomal after molecular simulation in vacuum.

$$\mathbf{E_{A\beta-Cu(II)}} = -133.51V_{\sum} = 3.24V_b + 58.12V_\theta + 15.14V_\varphi - 20.52V_{ij} - 4.25V_{hb} - 185.24V_{el}\ldots \quad (9)$$
$$\Delta\mathbf{E} = -2.122\ \text{kcal/mol}$$

$$\mathbf{E_{A\beta-Zn(II)}} = -137.07V_{\sum} = 3.23V_b + 58.15V_\theta + 15.07V_\varphi - 24.13V_{ij} - 4.24V_{hb} - 185.15V_{el}\ldots \quad (10)$$
$$\Delta\mathbf{E} = -5.683\ \text{kcal/mol}$$

$$\mathbf{E_{EDTA}} = 6.13V_{\sum} = 0.42V_b + 1.27V_\theta + 2.79V_\varphi + 1.65V_{ij}\ldots \quad (11)$$

$$\mathbf{E_{A\beta-Cu(II)-EDTA}} = -140.79V_{\sum} = 3.63V_b + 59.46V_\theta + 16.30V_\varphi - 31.30V_{ij} - 4.27V_{hb} - 184.61V_{el}\ldots \quad (12)$$
$$\Delta\mathbf{E} = -13.406\ \text{kcal/mol}$$

$$\mathbf{E_{A\beta-Zn(II)-EDTA}} = -135.42V_{\sum} = 3.59V_b + 59.87V_\theta + 18.66V_\varphi - 27.79V_{ij} - 4.43V_{hb} - 185.32V_{el}\ldots \quad (13)$$
$$\Delta\mathbf{E} = -4.476\ \text{kcal/mol}$$

Formation of the Nanoliposomal System

It is evident from the energy computations (Eqs. 3–7) that the nanoliposomal system was stabilized in terms of respective steric or potential energy factors. The preferred orientation of the polymers in the presence and absence of surfactant molecule is depicted in Fig. 9. Starting with a DSPE-PEG/DSPC binary system, the miscibility behavior of PC and DSPE-PEGs are known to be controversial for the formation of spherical particles since they are completely immiscible at all relevant pressures and compositions (47). In this study, we used 1,2 distearoyl-sn-glycero-3-phosphocholine with DSPE-PEG in order to form a stoichiometric condensed complex, DSPE-PEG/DSPC that is miscible with an energy stabilization of ΔE=−27.273 kcal/mol (Eqs. 3–5). The energy was mainly stabilized in terms of bond angles and torsional contributions (bonding energies) as well as London dispersion forces and H-bonding (non-bonding interaction). Among these forces, H-bonding stabilization was 40 times (due to the presence of the glycerol-functionality) greater than the combination which led to a stabilized molecular entity. Although, the blend was miscible, the formation of a liposomal system was still a challenge. To further increase the stabilization of the system, cholesterol (in excess) was introduced to act as filler in the space lattice of the binary system as shown in Fig. 9. This ternary system led to a super-stable molecular structure with a further decrease in constituent energies (Eqs. 6–7; ΔE= −79.786 kcal/mol) mainly in the form of van der Waals forces compared to H-bonding. This change in stabilization from H-bonding to van der Waals forces was due to hydrophobic interactions arising from the inclusion of cholesterol (overpowering the glycerol induced hydrophilic forces) leading to the formation of nanoliposomes in excess of phosphate buffered saline.

Energy Transformations Involving Metal Binding, Aggregation and Chelation

To study the effect of chelating agents, Aβ protein was individually modelled in conjugation with Cu(II) and Zn (II) followed by treating the energy minimized/stabilized molecular structures with EDTA (a metal chelator) as the prototype (Figs. 9 and 10). To increase the efficiency and selectivity of the computational process, we employed $A\beta_{10-21}$ (YEVHHQ KLVFFA) containing the His13 and His14 residues as a theoretical model variant instead of $A\beta_{1-42}$ (48). Systematic combination of the ligand atoms were

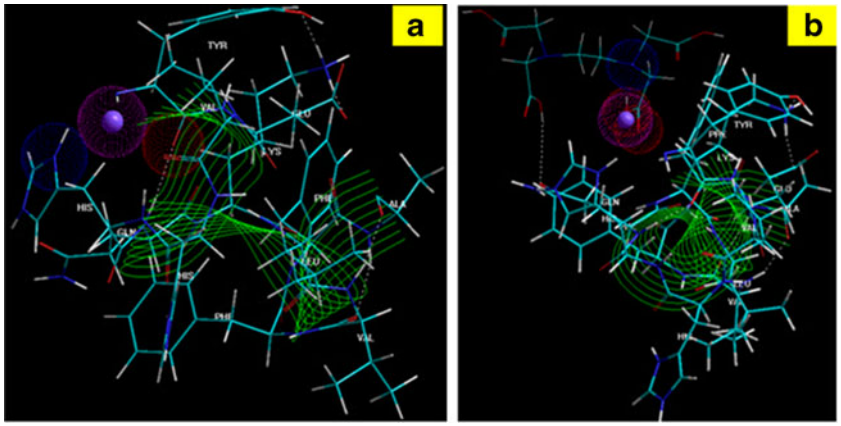

Fig. 10 Visualization of geometrical preferences of (**a**) Aβ(10-21)-Cu(II) and (**b**) Aβ(10-21)-Cu(II)-EDTA after molecular simulation in vacuum. Color codes: c (*cyan*), O (*red*), N (*blue*), P (*yellow*), H (*white*) and Cu (*violet*). Dots represent the overlapping van der Waals radii and the ribbon represents the secondary structure.

studied in several possible binding sites and modes for evaluating the optimum metal/protein energy minimized configurations of Cu(II)/Zn(II) binding to $A\beta_{10-21}$. The metal ions form close van der Waals space interactions with the Aβ protein, as depicted in Figs. 10a and 11a for Cu-Aβ and Zn-Aβ, respectively. The main region of interaction with minimized energy was His_{13}–Cu(II)/His_{13}–Zn(II) (with no H_2O molecules involved) which was in accordance with previously reported studies (49). Although, Zn(II) displayed a more stable protein complexation (Eqs. 8–10), both metal ions/protein interactions resulted in near equivalent minimization in potential energy ($\Delta E_{Cu\text{-}A\beta}$=−2.122 kcal/mol; $\Delta E_{Zn\text{-}A\beta}$=−5.683 kcal/mol) which was due to the close proximity of these metals within the periodic table and similar van der Waals radius. This observation was supported by the MMER analysis (Eqs. 8–10), where it was

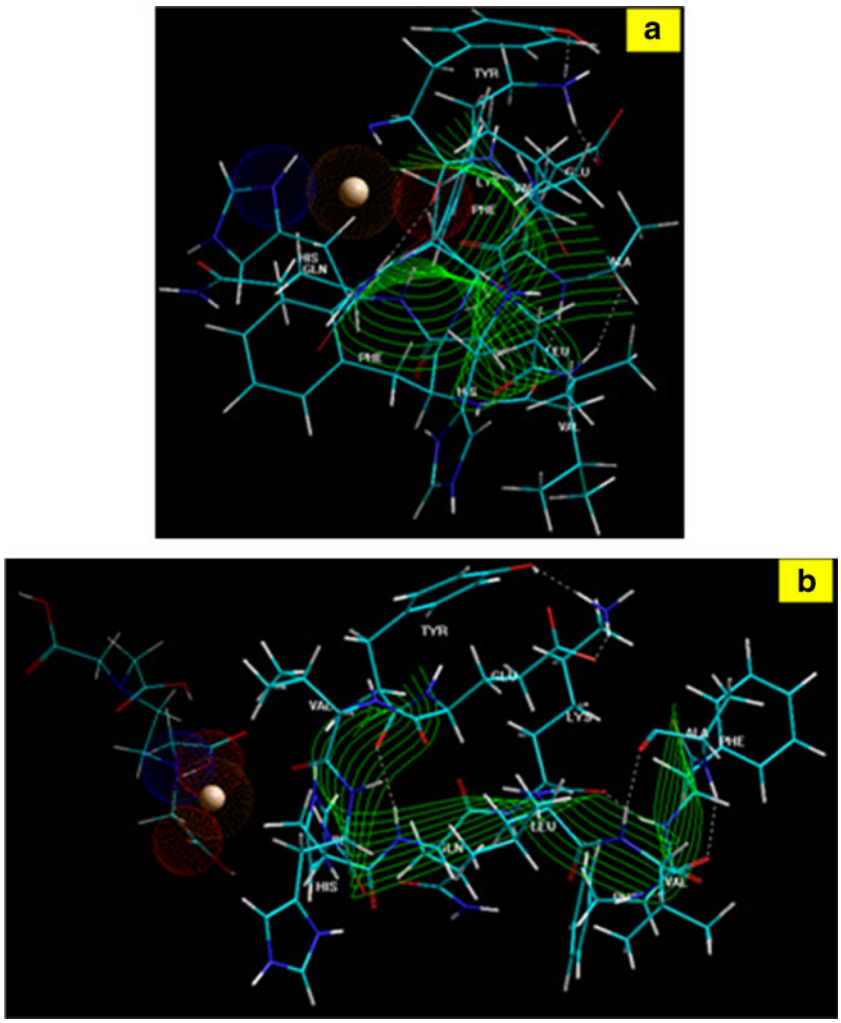

Fig. 11 Visualization of geometrical preferences of (**a**) Aβ(10-21)-Zn(II) and (**b**) Aβ(10-21)-Zn(II)-EDTA after molecular simulation in vacuum. Color codes: C (*cyan*), O (*red*), N (*blue*), P (*yellow*), H (*white*) and Zn (*brown*). Dots represent the overlapping van der Waals radii and the ribbon represents the secondary structure.

evident that London dispersion/van der Waals forces (hydrophobic interactions) led the entire energy minimization process.

The effect of adding a chelating agent on resolubilization of the aggregated Aβ protein (metal-induced aggregation) was modeled using EDTA as the prototype where a marked effect on the geometrical configuration of the metal/protein complex was observed. As soon as the EDTA molecule was in proximity of the van der Waals radius of the metal ion, it engulfed the metal ion with the so called "acetic acid claws". Interesting binding of the Aβ protein with EDTA in the case of Aβ-Cu(II)-EDTA confirmed the selectivity of Aβ towards the chelating agent in comparison to the metal ion which led to resolubilization. The stabilization in energies was not comparable with $\Delta E = -13.406$ kcal/mol and $\Delta E = -4.476$ kcal/mol in the case of Aβ-Cu(II)-EDTA and Aβ-Zn(II)-EDTA, respectively (Eqs. 11–13), respectively. This difference in energy was attributed to a decrease in dispersion forces and increased non-bonding interaction in the case of Aβ-Cu(II)-EDTA with the formation of H-bonds. In addition, close examination of the geometrical conformations clearly depicted the preference of metal ions towards EDTA (i.e. the chelating agents successfully extracted the metal ions from the Aβ-Cu(II)/Aβ-Zn(II) complex). This corroborates well with the observed *in vitro* experimental results where chelating ligand-bound modified NLPs modulated CuAβ(1-42)/ZnAβ(1-42) aggregates.

CONCLUSIONS

In this study, we confirmed the production of a new nano-liposomal chelator system after conjugating chelating ligands onto the surface of NLPs using either covalent or non-covalent conjugation procedures. The newly modified NLPs did not have a significant effect on the size of the NLPs compared with unmodified NLPs which makes them suitable for crossing the BBB. *In vitro* studies confirmed that the incubation of Cu(II) or Zn(II) with Aβ(1-42) peptide stimulated Aβ-aggregation. Modified NLPs (with EDTA, histidine and ZnAc) were suitable for resolubilization of CuAβ(1-42) and ZnAβ(1-42) aggregates *in vitro*. Furthermore, the high survival of PC12 neuronal cells after treatment with modified NLPs was influenced by inhibition of Aβ(1-42) aggregates, thereby protecting the cells from Aβ(1-42) aggregate related toxicity. High fluorescence microscopy also revealed that the modified NLPs in the presence of Zn (II) or Cu(II) was influenced by an ionophore process or macropinocytosis which is non-receptor mediated endocytosis or a biological metal ion pathway. The surface modified NLPs were able to protect PC12 neuronal cells from insoluble Aβ-peptides associated with neurotoxicity in AD. The *in vitro* studies were well corroborated by the *in silico* molecular mechanistic studies thus further confirming the potential of NLP/chelation therapy for AD.

REFERENCES

1. Cummings JH. Alzheimer's disease. N Engl J Med. 2004;351:56–67.
2. Brookmeyer R, Evans DA, Hebert L, *et al.* National estimates of the prevalence of Alzheimer's disease in the United States. Alzheimer's & Dementia. 2011;7:61–73.
3. Iversen LL, Mortishire-Smith RJ, Pollack SL, *et al.* The toxicity *in vitro* of beta-amyloid protein. Biochem J. 1995;311(1):1–16.
4. Marino T, Russo N, Toscano N, *et al.* On the metal ion (Zn(II), Cu (II)) coordination with beta-amyloid peptide: DFT computational study. Interdiscipl Sci. 2010;2:57–69.
5. De Strooper B, Annaert W. Proteolytic processing and cell biological functions of the amyloid precursor protein. J Cell Sci. 2000;113(11):1857–70.
6. Small DH, Mok SS, Bornstein JC. Alzheimer's disease and Aβ toxicity: from top to bottom. Nat Rev Neurosci. 2001;2(8):595–8.
7. Citron M. Beta-secretase as a target for the treatment of Alzheimer's disease. J Neurosci Res. 2002;70:373–9.
8. De Felice FG, Vieira MN, Saraiva LM, *et al.* Targeting the neurotoxic species in Alzheimer's disease: inhibitors of Aβ oligomerization. FASEB J. 2004;18:1366–72.
9. Lublin AL, Gandy S. Amyloid β oligemers: possible roles as key neurotoxicin in Alzheimer's disease. Mt Sinai J Med. 2010;77 (43):43–9.
10. Bush AI, Tanzi RE. Therapeutics for Alzheimers disease based on the metal hypothesis. Neurotherapeutics. 2008;5(3):421–32.
11. Lovell MA, Robertson JD, Teesdale WJ, *et al.* Copper, iron and zinc in Alzheimer's disease senile plaques. J Neurol Sci. 1998;158 (1):47–52.
12. Dong J, Atwood CS, Anderson VE, *et al.* Metal binding and oxidation of amyloid-beta within isolated senile plaque cores: Raman microscopic evidence. Biochem J. 2003;42:2768–73.
13. Duce JA, Bush AI. Biological metals and Alzheimer's disease: implications for therapeutics and diagnostics. Prog Neurobiol. 2010;92:1–18.
14. Zatta P, Drago D, Bolognin S, *et al.* Alzheimer's disease, metal ions and metal homeostatic therapy. Trends Pharmacol Sci. 2009;30 (7):346–55.
15. Opazo C. Transition metals and Alzheimer's disease. Rev Esp Geriatr Gerontol. 2005;40(6):365–70.
16. Bush AI. Metal complexing agents as therapies for Alzheimer's disease. Neurobiol Aging. 2002;23:1031–8.
17. Conway M, Holoman S, Jones L, *et al.* Selecting and using chelating agents. J Chem Eng. 1999;106(3):86–90.
18. Liu G, Men P, Kudo W, *et al.* Nanoparticle-chelator conjugates as inhibitors of Amyloid-β aggregation and neurotoxicity: a novel therapeutic approach for Alzheimer Disease. Neurosci Lett. 2009;455(3):187–90.
19. Seely DMR, Wu P, Mills EJ. EDTA chelation therapy for cardiovascular disease: a systematic review. BMC Cardiovasc. 2005;5 (32):1–6.
20. Nair NG, Perry G, Smith MA, *et al.* NMR studies of zinc, copper, and iron binding to histidine, the principal metal ion complexing site of amyloid-β peptide. J Alzheimer's Dis. 2010;20(1):57–66.
21. Chikha GG, Li WM, Schutze-Redelmeier MP, *et al.* Attaching histidine-tagged peptides and proteins to lipid-based carriers through use of metal-ion-chelating lipids. Biochim Biophys Acta. 2002;1567(1–2):204–12.

22. Marcellini M, Di Ciommo V, Callea F, *et al.* Treatment of Wilson's disease with zinc from the time of diagnosis in pediatric patients: a single-hospital, 10-year follow-up study. J Lab Clin Med. 2005;145 (3):139–43.
23. Shimizu N, Yamaguchi Y, Aoki T. Treatment and management of Wilson's disease. Pediatr Int. 1999;4(4):419–22.
24. Squitti R, Zito G. Anti-copper therapies in Alzheimer's disease: new concepts. Recent Pat CNS Drug Discov. 2009;4:209–19.
25. Popovic N, Brundin P. Therapeutic potential of controlled drug delivery systems in neurodegenerative diseases. Int J Pharm. 2006;314(2):120–6.
26. Cui Z, Lockman PR, Atwood CS, *et al.* Novel d-penicillamine carrying nanoparticles for metal chelation therapy in Alzheimer's and other CNS diseases. Eur J Pharm Biopharm. 2005;59:263–72.
27. Schnyder A, Huwyler J. Drug transport to brain with targeted liposomes. NeuroRx. 2005;2:99–107.
28. Liu GP, Men P, Harris PL, *et al.* Nanoparticle iron chelators: a new therapeutic approach in Alzheimer disease and other neurologic disorders associated with trace metal imbalance. Neurosci Lett. 2006;406:189–93.
29. Atyabi F, Farkhondehfa A, Esmaeili F, *et al.* Preparation of pegylated nano-liposomal formulation containing SN-38: *in vitro* characterization and *in vivo* biodistribution in mice. Acta Pharm. 2009;59:133–44.
30. Modi G, Pillay V, Choonara YE. Advances in the treatment of neurodegenerative disorders employing nanotechnology. Ann N Y Acad Sci. 2010;1184:154–72.
31. Kizelsztein P, Ovadia H, Garbuzenko O, *et al.* Pegylated nanoliposomes remote-loaded with the antioxidant tempamine ameliorate experimental autoimmune encephalomyelitis. J Neuroimmunol. 2009;213:20–5.
32. Yigit MV, Mishra A, Tong R, *et al.* Inorganic mercury detection and controlled release of chelating agents from ion-responsive liposomes. Chem Biol. 2009;16:937–42.
33. Phachonpai W, Wattanathorn J, Muchimapura S, *et al.* Neuroprotective effect of quercetin encapsulated liposomes: a novel therapeutic strategy against Alzheimer's disease. Am J Appl Sci. 2010;7(4):480–5.
34. Ying X, Wen H, Lu WL, *et al.* Dual-targeting daunorubicin liposomes improve the therapeutic efficacy of brain glioma in animals. J Contr Release. 2010;141:183–92.
35. Kamidate T, Hashimoto Y, Tani H, *et al.* Uptake of transition metal ions using liposome containing dicetylphosphate as a ligand. Anal Sci. 2002;18:273–6.
36. Suzuki R, Takizawa T, Negishi Y, *et al.* Gene delivery by combination of novel liposmal bubbles with perfluoropropane and ultrasound. J Contr Release. 2007;117:130–6.
37. Zhua J, Xue J, Guo Z, *et al.* Vesicle size and stability of biomimetic liposomes from 3′-Sulfo-Lewis a (SuLea)-containing glycolipids. Colloids Surf B Biointerfaces. 2007;58(2):242–9.
38. Verma DD, Verma S, Blume G, *et al.* Particle size of liposomes influences dermal delivery of substances into skin. Int J Pharm. 2003;258:141–51.
39. Yagi N, Ogawa Y, Kodaka M, *et al.* Preparation of functional liposomes with peptide ligands and their binding to cell membranes. Lipids. 2000;35:673–9.
40. Janssen AP, Schiffelers RM, ten Hagen TL, *et al.* Peptide-targeted PEG-liposome in anti-angiogenic therapy. Int J Pharm Pharm Sci. 2003;254(1):55–8.
41. Greene LA, Tischler AS. Establishment of a noradrenergic clonal line of rat adrenal pheochromocytoma cells which respond to nerve growth factor. PNAS. 1973;73:2424–8.
42. Zhang LW, Yang J, Barron AR, *et al.* Endocytic mechanisms and toxicity of a functionalized fullerene in human cells. Toxicol Lett. 2009;191:149–57.
43. Kumar P, Pillay V, Choonara YE, *et al.* In silico theoretical molecular modeling for Alzheimer's disease: the nicotine-curcumin paradigm in neuroprotection and neurotherapy. Int J Mol Sci. 2011;12:694–724.
44. Weers JG, Scheuing DR. Characterization of viscoelastic surfactant mixtures, I: fourier transform infrared spectroscopic studies. Colloids Surf B: Biointerfaces. 1991;1(55):41–56.
45. Strozyk D, Launer LJ, Adlard PA, *et al.* Zinc and copper modulate Alzheimer Aβ levels in human cerebrospinal fluid. Neurobiol Aging. 2009;30(7):1069–77.
46. Choonara YE, Pillay V, Ndesendo VMK, *et al.* Polymeric emulsion and crosslink-mediated synthesis of super-stable nanoparticles as sustained-release anti-tuberculosis drug carriers. Colloids Surf B: Biointerfaces. 2011;87:243–54.
47. Lozano MM, Longo ML. Microbubbles coated with disaturated lipids and DSPE-PEG2000: phase behavior, collapse transitions, and permeability. Langmuir. 2009;25:3705–12.
48. Morgan DM, Dong JJ, Jacob J, *et al.* Metal switch for amyloid formation: insight into the structure of the nucleus. J Am Chem Soc. 2002;124:12644–5.
49. Daxiong H, Haiyan W, Yang Y. Molecular modeling of zinc and copper binding with Alzheimer's amyloid b-peptide. Biometals. 2008;21:189–96.